

Nitrogen-doped graphene/carbon nanotube self-assembly for efficient oxygen reduction reaction in acid media

Chang Hyuck Choi^a, Min Wook Chung^b, Han Chang Kwon^a, Jae Hoon Chung^a, Seong Ihl Woo^{a,b,*}

^a Department of Chemical and Biomolecular Engineering, Korea Advanced Institute of Science and Technology, Daejeon 305-701, Republic of Korea

^b Graduate School of EWS (WCU), Korea Advanced Institute of Science and Technology, Daejeon 305-701, Republic of Korea

ARTICLE INFO

Article history:

Received 6 April 2013

Received in revised form 9 August 2013

Accepted 13 August 2013

Available online 22 August 2013

Keywords:

Oxygen reduction reactions

Graphene

Carbon nanotubes

Self-assembly

Nitrogen doping

ABSTRACT

Graphene, a two-dimensional layer structure of sp^2 -hybridized carbon, has garnered a great deal of attention as a promising material in electrochemistry. However, graphene has strong direction-dependent transport properties and is easily restacked to graphite; further development of graphene technology should thus be pursued for applications related to electrochemistry. Herein, a graphene/CNT self-assembly (GCA) was synthesized through the electrostatic interaction between graphene and CNTs, and was applied as a catalyst for oxygen reduction reactions (ORRs) in acid media after modification with N-doping. We demonstrated that the assembly with CNTs effectively increases the electric conductivity and hinders restacking of graphene layers, inducing facile transfer of electrons through CNTs and of reactants (e.g. oxygen and protons) through the interspace of graphene layers. The construction of highways for electrons and reactants on graphene layers resulted in 0.91 V onset potential and 2.13 mA/mg ORR activity at 0.75 V in acid media, representing significantly improved performance compared with that of catalysts derived from only graphene (0.86 V, 0.34 mA/mg) or CNTs (0.80 V, 0.02 mA/mg). In addition, the N-modified GCA shows much higher durability than that of only graphene, CNT or commercial Pt/C catalysts in severe operation conditions, with low production of peroxide in ORRs.

© 2013 Elsevier B.V. All rights reserved.

1. Introduction

Nitrogen-doped carbon materials with and without trace amounts of transition metals have been highlighted as non-precious metal catalysts for oxygen reduction reactions (ORRs) due to their high methanol/CO tolerance, good stability, and low price [1–11]. In alkaline media, various carbon materials reveal outstanding ORR performances which are comparable to that of a Pt catalyst [6–13]. However, the carbon materials unfortunately demonstrate much lower ORR activity compared to a Pt catalyst in acid media [1–5], which is the actual environment of polymer electrolyte membrane fuel cells (PEMFCs).

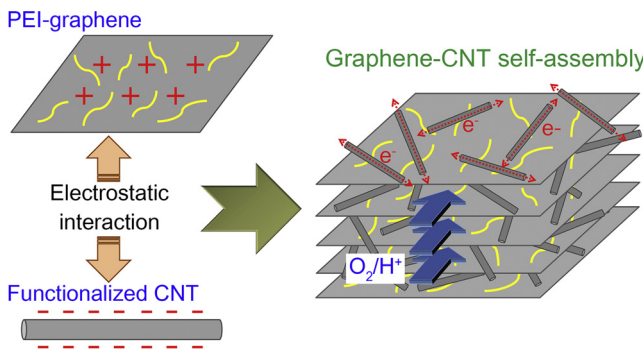
Since its discovery, graphene has enabled significant advancement of energy conversion and storage technologies due to its superior electrical and mechanical properties originating from the two-dimensional layered structure of sp^2 -hybridized carbon [14,15]. However, as a non-noble metal catalyst for ORRs in acid media, graphene-derived materials reveal no outstanding catalytic activity compared with those of other carbon-derived catalysts

[16–20]. Recently, through experimental and theoretical studies, Banks and coworkers proposed that graphene may not be a beneficial electrode material, as the large basal plane of graphene impedes efficient electron transfer and results in slow kinetics in electrochemical reactions [21]. Moreover, graphene layers are easily agglomerated and restacked by van der Waals interactions [22]. With respect to catalysis, restacking of graphene impedes facile transport of reactants between the graphene layers and reduces the number of active sites participating in the reaction, resulting in declined catalytic activity.

To secure high applicability of graphene as an electrode material, a graphene/CNT self-assembly (GCA) was developed and examined as a catalyst for ORRs in acid media after N-modification. Recently, Zhang et al. synthesized Fe-N doped CNT/graphene composite through growth of CNT on graphene layers, and reveals good ORR performance of the composite resulted from the uniform nucleation and growth of N-doped CNTs [23]. Contrary to the previous report, our strategy for graphene/CNT self-assembly centered on the deposition of CNTs on the graphene layers; thus, in the assembly, CNTs act as circuits for facile electron transfer and as spacers for preventing restacking of graphene layers, introducing interlayer spaces for effective transport of the reactants ([Scheme 1](#)). Similar methods have been explored in the area of

* Corresponding author. Tel.: +82 42 350 3958.

E-mail address: siwoo@kaist.ac.kr (S.I. Woo).



Scheme 1. Strategy for enhancing the applicability of graphene as an electrode material.

super-capacitors [24–27], but we examined this strategy for application of graphene as an electro-catalytic material toward ORRs in acid media. Self-assembly was performed by electrostatic interaction between poly-ethyleneimine (PEI)-modified graphene having a positive charge and acid-treated CNT having a negative charge [28]. The PEI-modified graphene was synthesized from graphite oxide (GO, Fig. S1). For application as ORR catalysts, N was doped into the prepared carbon materials through pyrolysis with dicyanodiamide and small amounts of transition metal chlorides (Co and Fe), followed by acid-treatment to eliminate the metals [19,29]. Finally, three-different catalysts were obtained: N-doped CNTs (NCNT), N-doped graphene (NGr), and N-doped GCA (NGCA).

2. Experimental

2.1. Preparation of GO, graphene, and GCA, and N-modifications

All chemicals were obtained from Aldrich. The GO was prepared by using methods reported elsewhere [30]. Briefly, graphite (3 g) was dispersed in a concentrated acid mixture of H_2SO_4 and H_3PO_4 . After the addition of $KMnO_4$ (18 g), the solution was heated at 50 °C for 12 h. The solution was poured onto ice (400 mL), and then H_2O_2 (5 mL) was added. The GO was obtained after an iterative centrifuge with a HCl solution and deionized (DI) water. The graphene was synthesized by reduction of GO (0.2 g) with hydrazine (0.6 mL) as reducing agent at 95 °C.

Self-assembly of graphene and CNTs was performed by electrostatic interaction between surface modified graphene and CNTs [28]. The graphene surface was modified with poly(ethyleneimine). The GO (0.2 g) was dispersed by ultra-sonication in DI-water (200 mL). After the addition of PEI solution (50 wt.%, 6 g), the GO solution was stirred at 60 °C for 12 h. After cooling the solution to room temperature, GO was reduced by the same procedure as employed for graphene. The surface of CNTs (0.5 g) was acid-treated with concentrated H_2SO_4 (150 mL) and HNO_3 (50 mL) at 70 °C for 90 min. For self-assembly, surface modified graphene and CNTs (graphene: CNTs = 3:1 wt. ratio) were well-dispersed in 200 mL of DI-water by ultra-sonication for 1 h, and then self-assembly proceeded under stirring for 1 h. The GCA was finally obtained by centrifugation, washing with DI-water, and drying in a vacuum oven.

During the synthesis procedures, hydrazine was used as reducing agent but it was also able to act as N-doping source in the reaction. However, the effect of hydrazine on the ORR activity of carbon material is not significant and further N-modification step should be followed [31]. N-modification of the CNTs, graphene, and GCA was performed by pyrolysis of a mixture of carbon-material (0.2 g), $CoCl_2 \cdot 6H_2O$ (2 mg), $FeCl_2 \cdot 4H_2O$ (5 mg), and DCDA (0.4 g). It is well known that the presence of trace amount of metal in pyrolysis step assist generation of highly active

carbon-derived catalysts for ORRs in acid media [32]. All precursors were dissolved in DI-water (50 mL), and sonicated for 1 h. A solid mixture was obtained after evaporation of the solution, and the powder was heat-treated at 900 °C for 3 h under an Ar atmosphere. Acid leaching was conducted in a H_2SO_4 solution (0.5 M, 100 mL) for 8 h at 80 °C to dissolve acid-unstable metal phases. Finally, this procedure was conducted once again.

2.2. Physical characterizations

The physical properties of the graphene-derived catalysts were examined via four-point probe, X-ray diffraction (XRD), transmission electron microscopy (TEM), scanning electron microscopy (SEM), Raman spectroscopy, X-ray photoelectron spectroscopy (XPS), element analysis (EA), and inductively coupled plasma (ICP).

The sheet resistivity of carbon film was obtained by a CMT-SR2000NW (Advanced Instrument Technology). The carbon film was prepared on a slide glass substrate by spraying carbon-polytetrafluoroethylene (PTFE) ink (Carbon: PTFE = 3 wt.:1 wt.). The XRD patterns were acquired from a D/MAX-2500 (Rigaku) operated at 40 kV and 300 mA with $Cu K\alpha$ as a X-ray source. The step-scan patterns were collected in a range of 2° to 60° (2θ ranges) with a step size of 0.01° and a scan speed of 1° min^{-1} . The TEM and SEM images were taken with a HD-2300A (Hitachi) operated at 200 kV. Raman spectroscopy was performed using LabRAM HR UV-vis/NIR (Horiba Jobin Yvon) with a laser source of 514 nm. The XPS analysis was performed using a Sigma Probe (Thermo VG Scientific) equipped with a microfocused Al monochromator X-ray source. XPS-N_{1s} peaks were deconvoluted by pyridinic-N (398.6 eV), graphitic- or pyrrolic-N (401 ± 0.5 eV), and pyridinic-oxide (403 eV). The compositions of the prepared catalysts were obtained from an EA using a FlashEA 1112 and from an ICP analysis using a POLY SCAN 61 E.

2.3. Electrochemical characterizations

The electrochemical properties were characterized using a CHI700D (CH Instruments Inc.) and a RRDE-3A (ALS Co.) in a three-electrode beaker cell equipped with a Pt wire counter electrode (ALS Co., 002233), an Ag/AgCl reference electrode (ALS Co., 012167), and a ring disk electrode (ALS Co., 011169). The catalysts (10 mg) were dispersed in a Nafion ink solution (1 mL, 1 wt.% Nafion content), and then ink (5 μ L) was dropped onto the glassy carbon (3 mm) of the ring disk electrode. The inks were dried at room temperature. Loading amount of the catalysts was 714 μ g/cm². Cyclic voltammetry (CV) was conducted in a 1 M $HClO_4$ electrolyte purged with nitrogen or oxygen for more than 1 h, with a 40 mV/s scan rate from -0.22 to 1 V (vs. Ag/AgCl). The specific capacitance was obtained from the CV result in nitrogen-purged 1 M $HClO_4$ electrolyte by using the following equation:

$$C = \frac{\int Idt}{m\Delta V} \quad (1)$$

where C is the specific capacitance, I is the current from CV result, t is the time, m is the mass of the carbon material, and ΔV is the potential range.

Linear sweep voltammetry (LSV) was performed in a 1 M $HClO_4$ electrolyte purged by nitrogen or oxygen with a 5 mV/s scan rate from 0.82 to -0.08 V (vs. Ag/AgCl) and 2000 rpm rotation speed. The ORR currents were obtained by subtracting the LSV results for the nitrogen-purged electrolyte from those of the oxygen-purged electrolyte, in order to remove the capacitance of the catalysts. A Tafel-plot based on kinetic current in ORRs and ORR pathway was obtained by using Koutecky-Levich's equation:

$$\frac{1}{I} = \frac{1}{I_k} + \frac{1}{I_d} + \frac{1}{I_k} + \frac{1}{0.62nFDA_{O_2}^{2/3} v^{-1/6} C_0 \omega^{1/2}} \quad (2)$$

where I is the measured current, I_k is the kinetic current, I_d is the diffusion current, n is the number of electrons involved in ORRs, F is Faraday constant ($96,485 \text{ C mol}^{-1}$), A is the geometric electrode area, D is the diffusion coefficient of O_2 ($1.9 \times 10^{-5} \text{ cm}^2/\text{s}$ in 1 M HClO_4), ν is the kinetic viscosity of solution ($9.87 \times 10^{-3} \text{ cm}^2/\text{s}$), C is the saturation concentration of O_2 ($1.6 \times 10^{-3} \text{ mol/L}$), and $\omega = 2\pi f/60$ is the angular rotation speed (rad/s , f is electrode rotation speed in rpm). Electrochemical impedance study of NGCA was performed in oxygen-saturated 1 M HClO_4 solution with the frequency range from 10 kHz to 0.1 Hz .

The H_2O_2 formation yield was derived from the current at the rotated Pt-ring disk electrode (RRDE) applied to 1 V (vs. Ag/AgCl) of constant potential, and the following equation was used:

$$\text{H}_2\text{O}_2(\%) = 200 \times \frac{I_R/N}{I_R/N + I_D} \quad (3)$$

$$n = 4 \times \frac{I_D}{I_R/N + I_D} \quad (4)$$

where I_R is the ring current, I_D is the disk current, N is the collection efficiency (0.37), and n is the number of electrons transferred in ORRs.

All potentials shown in this paper were converted to the reversible hydrogen electrode (RHE) scale. The current-time chronoamperometric response was obtained at 0.38 V (vs. Ag/AgCl) for 10 h in 1 M HClO_4 with continuous oxygen bubbling and commercial Pt/C (20 wt.%, E-tek, loading amount = $20 \mu\text{g of Pt/cm}^2$) was used for comparison.

3. Results and discussion

3.1. Electron conductivities of the prepared catalysts

The electron transfer ability of the prepared carbon materials was examined and is indicated by sheet resistivity in Fig. 1. CNTs are a good electron-conductive material with low sheet resistivity, but graphene shows relatively high sheet resistivity. This result is consistent with a previous report that low electron conductivity could be observed in graphene due to its strong direction-dependent electrical transport property (extremely low out-of-plane conductivity) [25], and low electron density on the large basal plane [21]. However, the sheet resistivity of graphene is effectively decreased through decoration with CNTs (GCA), which act as tunnels for facile transfer of electrons.

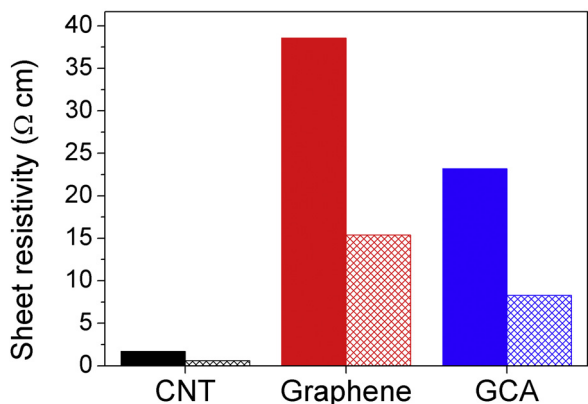


Fig. 1. Sheet resistivities of the prepared carbon films. Filled and patterned bars indicate sheet resistivities of bare and N-doped carbon materials, respectively.

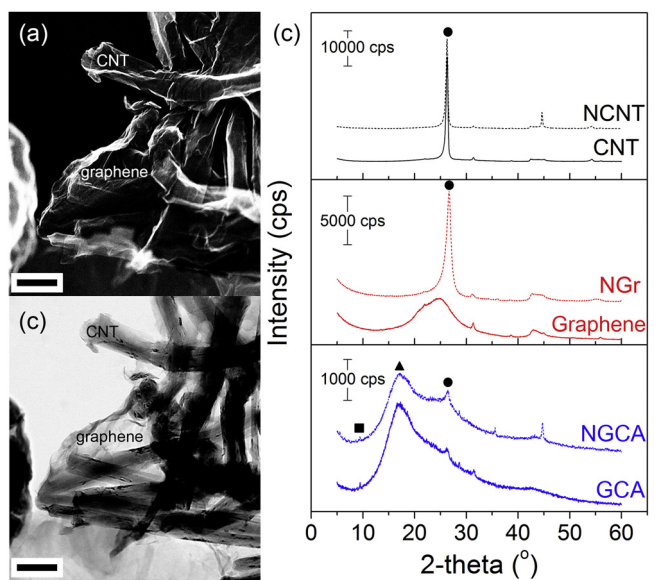


Fig. 2. (a) SEM and (b) TEM images of the GCA (Scale bar = 300 nm). (c) XRD results of all the prepared materials.

3.2. Morphologies of the prepared catalysts

SEM and TEM images of GCA in Fig. 2a and b show that CNTs are randomly deposited on the graphene surface, indicating a self-assembled structure of GCA. As shown in Fig. 2c, graphene synthesized by reduction of GO has broad peaks near 24.9° with 3.57 \AA interlayer distance. This broad peak emerges due to the removal of oxygen atoms from GO and random rearrangement of graphene layers to the graphite gallery [33]. However, after N-modification at 900° C , an intense graphite peak at 26.5° (denoted with circles in Fig. 2c) with 3.33 \AA interlayer distance is obtained in XRD patterns, similar with the XRD patterns of CNTs and NCNTs. The newly generated graphite peaks in the XRD results of NGr reveal that the graphene is restacked, resulting in graphite structures. Interestingly, XRD patterns of GCA show a very broad peak at 16.9° (denoted by a triangle in Fig. 2c), and a peak at 9.7° (denoted by a rectangle in Fig. 2c), as also observed in the XRD results of GO (Fig. S1b). Moreover, contrary to graphene, the XRD results of GCA and NGCA have similar patterns, indicating no alteration of GCA interlayer distance after N-modification steps. A slight graphite peak is observed in both GCA and NGCA, but this is due to the presence of a small amount of CNTs (25 wt.%). The interspace distances of GCA are 5.16 \AA , and 9.35 \AA , calculated from the peaks at 16.9° and 9.7° , respectively, and these distances are much longer than that of graphene (3.57 \AA). The results demonstrate that the CNTs in the GCA play a role as a spacer, which increases the interlayer distances, and an inhibitor in the restacking of graphene. This finding, the prohibition of graphene restacking through the assembly with CNTs, is also supported by Raman spectroscopy of NGr and NGCA (Fig. S2). A relatively broad 2D-band peak was observed for NGr, but NGCA shows a sharp and intense 2D-band peak. This indicates that NGr consists of several layers of graphene sheets, which results from restacking of graphene through N-modification steps; this phenomenon is, however, effectively regulated by the assembly of graphene and CNTs [34].

Fig. 3

3.3. Catalyst compositions and N-doping phases

The bulk compositions of the prepared N-modified carbons are listed in Table S1. To monitor the doping of nitrogen, an XPS analysis

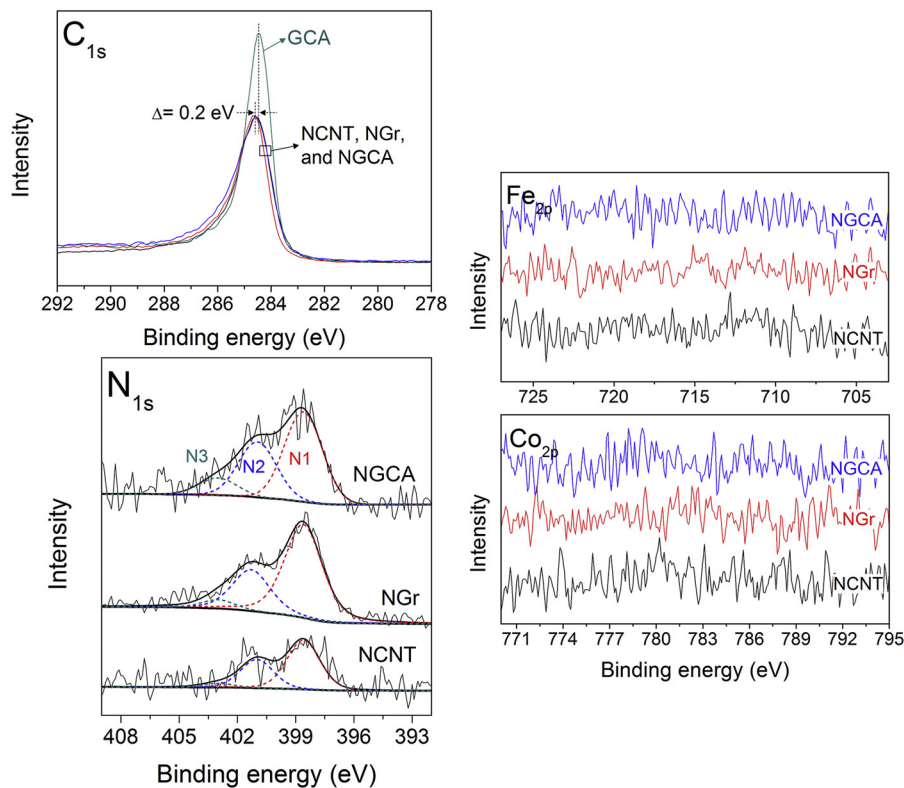


Fig. 3. XPS-C_{1s}, -N_{1s}, -Fe_{2p}, and -Co_{2p} measurements of the prepared carbon materials. XPS-N_{1s} results were deconvoluted by pyridinic-N (N1), graphitic- or pyrrolic-N (N2), and pyridinic-oxide (N3).

for the prepared carbon materials was carried out and the results are shown in Figs. 3 and S3. The surface compositions of the prepared materials obtained from XPS results were organized in Table S2. Generally, the binding energy of C–C bonding for bare graphite emerges at 284.5 eV [35], but all of the prepared N-modified carbon materials reveal a 0.2 eV up-shift of the binding energy to 284.7 eV. Up-shift of the binding energy for C–C bonding was also observed in other N-doped carbon materials reported elsewhere [36–38], and is due to charge-delocalization derived by the higher electronegativity of N [19]. As shown in the XPS-N_{1s} results, N is doped into the carbon materials in various forms: pyridinic-N (N1), graphitic- or pyrrolic-N (N2), and pyridinic-oxide (N3) [32]. Regardless of the carbon morphologies, all of the N-modified carbons show similar shapes in terms of XPS-N_{1s} peaks and pyridinic-N is the dominant site. In addition, the absence of peaks in XPS-Fe_{2p} and -Co_{2p} indicates that contents of remaining metal phases are lower than detection limit of XPS instruments (>1 at.%) after acid-leaching steps, and it is confirmed by ICP analysis (Table S1, metal contents < 0.21 at.%).

3.4. ORR activities and stabilities of the prepared catalysts

As electro-catalytic materials for ORRs in acid media, the CV of the prepared carbons was examined in N₂- and O₂-bubbled 1 M HClO₄ electrolytes (Fig. S4). Specific capacitances obtained from the CV results in N₂-bubbled 1 M HClO₄ electrolyte were 17.6, 114.5, and 181.6 F/g at a scan rate of 40 mV/s for NCNT, NGr, and NGCA, respectively. Specific capacitance is proportional to the electrochemically accessible surface area of the carbon materials [39], thus it indicates that assembled structure increases efficient mass/charge transport through the interlayer space of graphenes due to the presence of CNTs between the graphene layers. The results show significant reduction currents of CV curves under the

O₂-bubbled electrolyte, indicating good ORR ability of the prepared carbons. The reduction-peak potentials (Fig. S4d) of the NCNT, NGr, and NGCA were 0.37, 0.51, and 0.66 V (vs. RHE) with –1.59, –3.74, and –4.49 mA/cm² of peak current densities, respectively. NGCA showed the highest reduction-peak potentials, indicating that it had the highest ORR activity among the prepared materials.

To obtain more detailed electrochemical properties, LSV was performed in O₂-bubbled 1 M HClO₄ solutions with 2000 rpm electrode rotation speed, and kinetic currents were shown as the Tafel-plots. As shown in Fig. 4a and b, NGCA displays an onset potential (vs. RHE) of approximately 0.91 V, which is much higher than those of NCNT (0.8 V) and NGr (0.86 V). Moreover, NGCA shows much higher current density obtained from ORRs compared to NCNT and NGr. Before heat-treatment with DCDA and metal chlorides, GCA shows much lower ORR activity in acid media than that of NGCA. This indicates that heat-treatment step effectively generates ORR active sites on the GCA. The mass activities of NCNT and NGr at 0.75 V (vs. RHE) are 0.02 and 0.34 mA/mg, respectively. As observed in Fig. 4c, NGCA results in more than six-fold higher mass activity (2.13 mA/mg) compared to that of NGr. Even though it is hard to compare ORR activity directly to the results obtained from other groups due to different experimental conditions, NGCA demonstrates outstanding ORR performance among other graphene-derived catalysts reported elsewhere (Table S3). However, this activity is still lower than that of Pt/C.

The stability of the prepared carbon was examined by current-time chronoamperometric measurement at 0.6 V for 10 h in a 1 M HClO₄ solution with continuous O₂-bubbling (Fig. 4d and Fig. 5a). After 10 h of operation, performance degradation of NGCA was –23.3%, but that of NCNT, NGr, and Pt/C was –42.3, –42.0, and –57.3%, respectively, demonstrating high stability of NGCA in acid media.

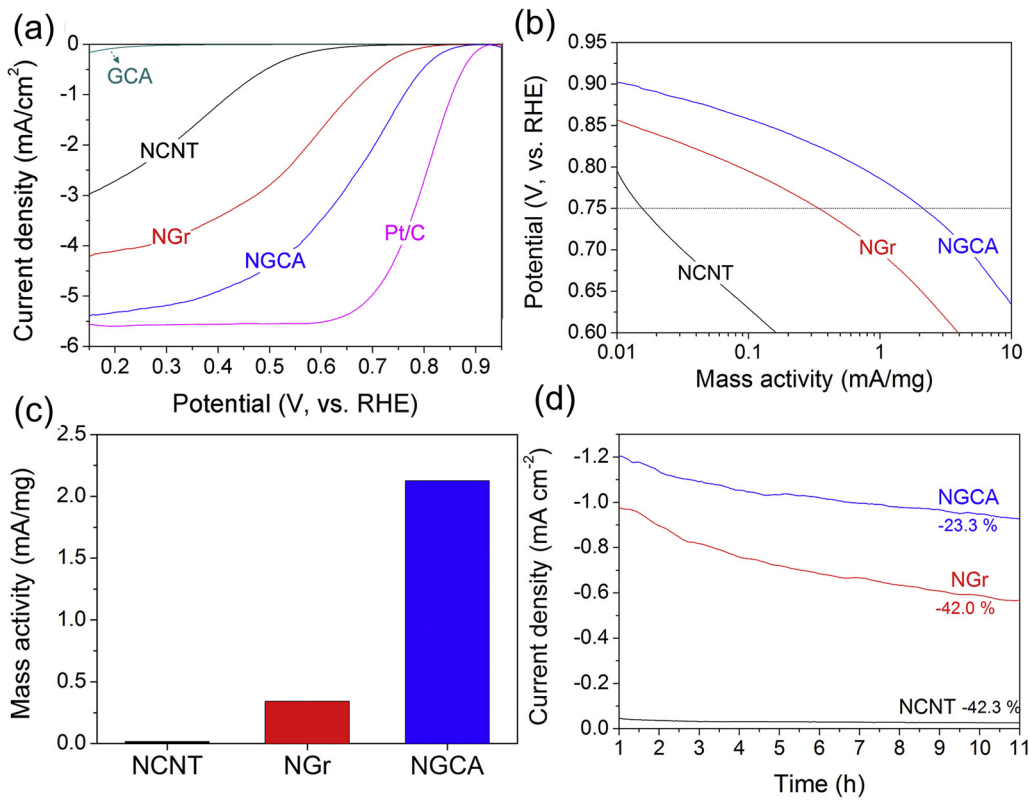


Fig. 4. (a) LSV curves in O₂-bubbled 1 M HClO₄ solutions with 2000 rpm of electrode rotation speed, (b) Tafel-plots based on unit mass of the carbons, (c) mass activities (mA/mg) calculated at 0.75 V (vs. RHE), and (d) current–time chronoamperometric responses obtained at 0.6 V (vs. RHE) for 10 h.

3.5. Origin of enhanced ORR activity of the NGCA

Bulk (Table S1) and surface compositions (Table S2) of the prepared catalysts indicates that N-content increases in the order of NCNT, NGr, and NGCA, and this order is corresponded well with the order of ORR activity. However, it was revealed that N-content has minor effects on ORR performance in acid media [1]. Therefore, it is supposed that other characteristics (e.g. electron/mass transport) determine the ORR activity in this case.

Although the active sites in these types of catalysts were very controversial topics (e.g. metal nitrogen complex [3,23,40] or charge/spin-localized carbon atoms [41–43]), the ORRs are carried out where the triple phase boundary is constructed, which accompanies collisions among oxygen molecules, protons, and electrons and produces water molecules. Thus, efficient transport of these reactant molecules and electrons to the active sites of the catalysts is responsible for the high ORR performance. However, graphene prepared by chemical reduction of GO usually shows much lower electron conductivity (nearly 100–200 S/m) than that of CNTs (usually 10,000 S/m) [26]. Moreover, strong van der Waals interactions between graphene layers lead to graphene-restacking [22], and result in the decrement of the interlayer distance, through which oxygen and protons cannot be transported.

In the case of GCA, an assembled structure of graphene and CNTs, significant improvement in the ORRs is due to enhanced transport of the reactant molecules and electrons to the active sites on the catalyst. As mentioned above, assembly of CNTs on the graphene layers reduces the electrical resistivity (Fig. 1), and also prevents restacking of graphene layers even after heat-treatment steps for N-modification (Figs. 2 and S2). Moreover, electrochemical impedance spectroscopic (EIS) Nyquist plots (Fig. 5b), which were obtained in O₂-saturated 1 M HClO₄, show smaller semi-circle response for NGCA than that for NGr, indicating improved

electron/mass transfer ability in NGCA during the ORRs. This result is consistent with the previous reports that CNTs presented in the graphene layers can act as tunnels for fast electron transfer and as spacers for efficient diffusion of reactant molecules [24–27], thereby facilitating enhanced ORRs.

3.6. Low production of H₂O₂ in ORRs for NGCA

Moreover, the graphene/CNT self-assembled structure also modified the ORR pathways. The production of H₂O₂, a byproduct of ORRs that attacks fuel cell systems and leads to performance degradation [44], is obtained from RRDE analysis and shows 21% for NCNT ($n = 3.58$; “ n ” is the number of electrons transferred in the ORRs) and 15% for NGr ($n = 3.70$), respectively; however, it effectively decreases to nearly 3% for NGCA ($n = 3.94$), indicating it has nearly a 4-electron pathway in ORRs (Fig. 5c). Moreover, the number of electrons transferred in ORRs obtained from the Koutecky-Levich plot are from 3.78 to 3.93 in the potential range from 0.65 V to 0.5 V (Fig. 5d), indicating the dominant 4-electron ORR pathway for NGCA. Kurak and Anderson simulated oxygen reduction on N-doped graphene models on the basis of density functional theory (DFT) studies [45], and revealed a dominant two-electron pathway producing H₂O₂ in ORRs when the oxygen molecules are adsorbed at the edge of the graphene (path-I). On the other hand, Zhang and Xia demonstrated a dominant four-electron pathway in ORRs for N-doped graphene [41]. According to their DFT calculations, oxygen molecules are adsorbed on the carbon atoms on the basal plane of graphene, which has the highest spin or charge density (not the edge sites of graphene). The graphene layer is then deformed by the chemical bond between O and C atoms, which results in a tetrahedral structure out of the graphene plane during the ORRs (path-II).

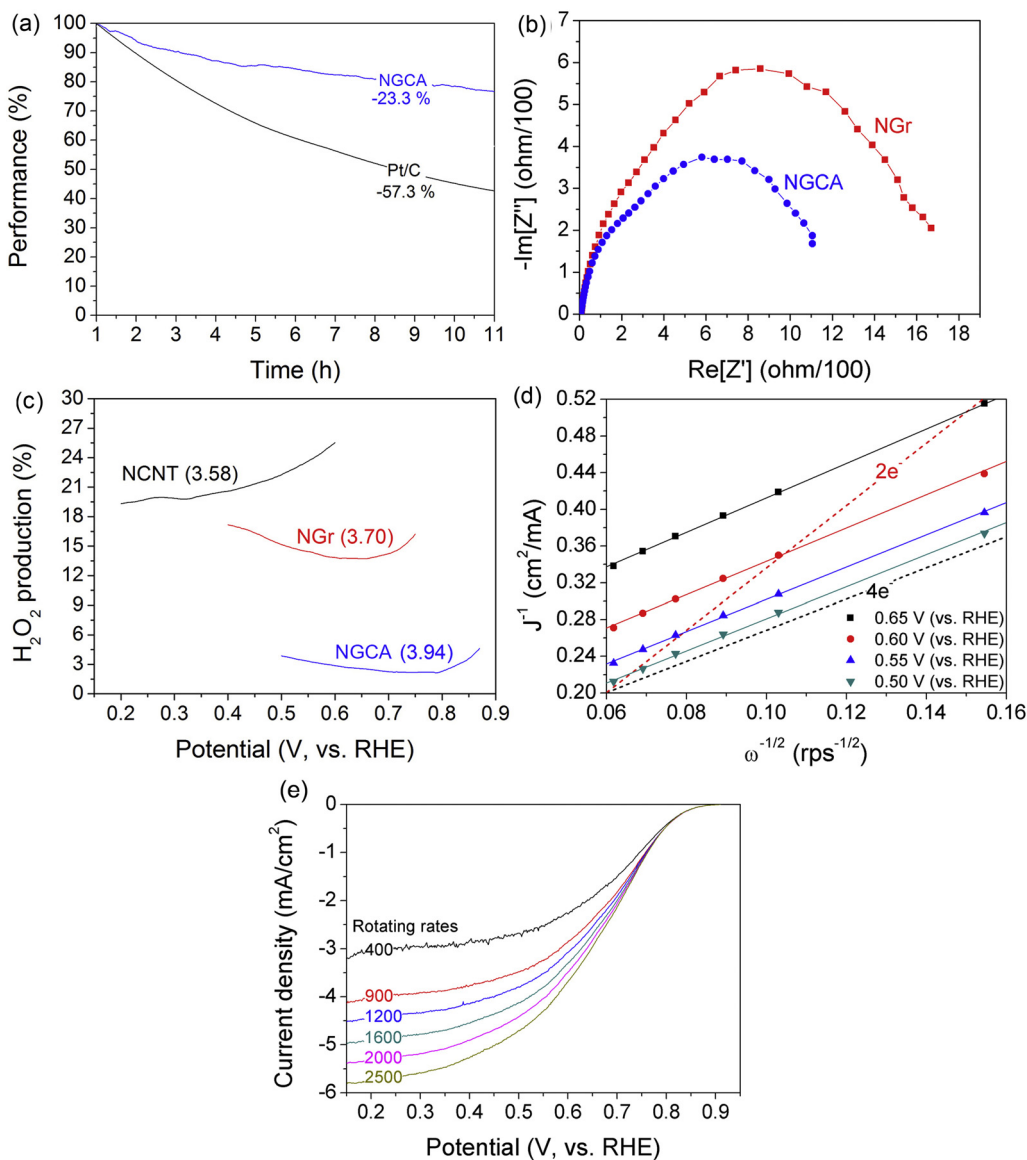


Fig. 5. (a) Current–time chronoamperometric responses of NGCA and Pt/C catalysts obtained at 0.6 V (vs. RHE) for 10 h, and (b) electrochemical impedance spectroscopic Nyquist plots measured for NGr and NGCA in oxygen-saturated 1 M HClO_4 with the frequency range from 10 kHz to 0.1 Hz. (c) H_2O_2 production yields calculated by currents from the ring disk electrode. The values in parentheses indicate the average number of electrons transferred. (d) Koutecky–Levich plots for NGCA at different potentials. (e) ORR polarization plots of NGCA catalyst in O_2 -saturated 1 M HClO_4 electrolytes at different rotation rates.

In NGr, single graphene layers are stacked on top of one another and it has a very short interlayer distance similar to that of graphite (Fig. 2c). Thus, many oxygen molecules are adsorbed at the edge of the graphene layers and a large quantity of peroxide is produced (path-I). However, NGCA shows a longer interlayer distance than that of NGr, and is relatively free from adsorption of oxygen molecules at carbon atoms on the basal plane of graphene and from deformation out of the graphene plane derived by oxygen-chemisorption. Oxygen molecules are thus easily reduced by the path-II mechanism on NGCA, resulting in decrement of H_2O_2 production.

4. Conclusions

To improve the ORR activity of graphene materials, a graphene/CNT self-assembly was prepared by the electrostatic interaction between graphene and CNTs, and was doped with nitrogen by pyrolysis of dicyandiamide. The CNTs act as

highways for facile electron transfer and as spacers for hindering graphene-restacking in the assembled structure, resulting in efficient transport of reactant molecules and electrons. They also provide sufficient space for graphene-deformation that derived from oxygen-chemisorption on the basal plane of the graphene layer. NGCA shows 2.13 mA/mg of ORR activity at 0.75 V in acid media, which is more than six-fold higher than that of NGr. In addition to high activity, NGCA displays high stability in acid media with an enhanced 4-electron pathway in ORRs. The results reveal that self-assembled structure of graphene and CNTs are favorable for the ORRs in acid media, thus we believe this assembly is potentially one of the promising alternative materials as a cathode electrode for fuel cell applications.

Acknowledgment

This work was supported by the National Research Foundation of Korea (NRF) grant funded by the Korea government (MEST) (No. 2009-0092783).

Appendix A. Supplementary data

Supplementary data associated with this article can be found, in the online version, at <http://dx.doi.org/10.1016/j.apcatb.2013.08.021>.

References

- [1] F. Jaouen, J. Herranz, M. Lefevre, J.P. Dodelet, U.I. Kramm, I. Herrmann, P. Bogdanoff, J. Maruyama, T. Nagaoka, A. Garsuch, J.R. Dahn, T. Olson, S. Pylypenko, P. Atanassov, E.A. Ustinov, *ACS Appl. Mater. Interfaces* 1 (2009) 1623–1639.
- [2] G. Liu, X.G. Li, J.W. Lee, B.N. Popov, *Catal. Sci. Technol.* 1 (2011) 207–217.
- [3] Y. Li, W. Zhou, H. Wang, L. Xie, Y. Liang, F. Wei, J.C. Idrobo, S.J. Pennycook, H. Dai, *Nat. Nanotechnol.* 7 (2012) 394–400.
- [4] M. Lefevre, E. Proietti, F. Jaouen, J.P. Dodelet, *Science* 324 (2009) 71–74.
- [5] G. Wu, K.L. More, C.M. Johnston, P. Zelenay, *Science* 332 (2011) 443–447.
- [6] K. Parvez, S. Yang, Y. Hernandez, A. Winter, A. Turchanin, X. Feng, K. Müllen, *ACS Nano* 6 (2012) 9541–9550.
- [7] D. Deng, L. Yu, X. Chen, G. Wang, L. Jin, X. Pan, J. Deng, G. Sun, X. Bao, *Angew. Chem. Int. Ed.* 52 (2013) 371–375.
- [8] J. Liang, Y. Jiao, M. Jaroniec, S.Z. Qiao, *Angew. Chem. Int. Ed.* 51 (2012) 11496–11500.
- [9] D. Geng, Y. Chen, Y. Chen, Y. Li, R. Li, X. Sun, S. Ye, S. Knights, *Energy Environ. Sci.* 4 (2011) 760–764.
- [10] L.F. Lai, J.R. Potts, D. Zhan, L. Wang, C.K. Poh, C.H. Tang, H. Gong, Z.X. Shen, L.Y. Jianyi, R.S. Ruoff, *Energy Environ. Sci.* 5 (2012) 7936–7942.
- [11] K. Gong, F. Du, Z. Xia, M. Durstock, L. Dai, *Science* 323 (2009) 760–764.
- [12] M. Vikkisk, I. Kruusenberg, U. Joost, E. Shulga, K. Tammeveski, *Electrochim. Acta* 87 (2013) 709–716.
- [13] N. Alexeyeva, E. Shulga, V. Kisand, I. Kink, K. Tammeveski, *J. Electroanal. Chem.* 648 (2010) 169–175.
- [14] D. Chen, L.H. Tang, J.H. Li, *Chem. Soc. Rev.* 39 (2010) 3157–3180.
- [15] Y.Q. Sun, Q.O. Wu, G.Q. Shi, *Energy Environ. Sci.* 4 (2011) 1113–1132.
- [16] K.R. Lee, K.U. Lee, J.W. Lee, B.T. Ahn, S.I. Woo, *Electrochim. Commun.* 12 (2010) 1052–1055.
- [17] C.W. Tsai, M.H. Tu, C.J. Chen, T.F. Hung, R.S. Liu, W.R. Liu, M.Y. Lo, Y.M. Peng, L. Zhang, J.J. Zhang, D.S. Shy, X.K. Xing, *RSC Adv.* 1 (2011) 1349–1357.
- [18] C. Arizzani, S. Righi, F. Soavi, M. Mastragostino, *Int. J. Hydrogen Energy* 36 (2011) 5038–5046.
- [19] J.Y. Choi, D. Higgins, Z.W. Chen, *J. Electrochem. Soc.* 159 (2012) B87–B90.
- [20] H.R. Byon, J. Suntivich, Y. Shao-Horn, *Chem. Mater.* 23 (2011) 3421–3428.
- [21] D.A.C. Brownson, L.J. Munro, D.K. Kampouris, C.E. Banks, *RSC Adv.* 1 (2011) 978–988.
- [22] J. Yan, T. Wei, B. Shao, F.Q. Ma, Z.J. Fan, M.L. Zhang, C. Zheng, Y.C. Shang, W.Z. Qian, F. Wei, *Carbon* 48 (2010) 1731–1737.
- [23] S. Zhang, H. Zhang, Q. Liu, S. Chen, *J. Mater. Chem. A* 1 (2013) 3302–3308.
- [24] Y. Wang, Y.P. Wu, Y. Huang, F. Zhang, X. Yang, Y.F. Ma, Y.S. Chen, *J. Phys. Chem. C* 115 (2011) 23192–23197.
- [25] F. Du, D.S. Yu, L.M. Dai, S. Ganguli, V. Varshney, A.K. Roy, *Chem. Mater.* 23 (2011) 4810–4816.
- [26] Q. Cheng, J. Tang, J. Ma, H. Zhang, N. Shinya, L.C. Qin, *Phys. Chem. Chem. Phys.* 13 (2011) 17615–17624.
- [27] N. Jha, P. Ramesh, E. Bekyarova, M.E. Itkis, R.C. Haddon, *Adv. Energy Mater.* 2 (2012) 438–444.
- [28] D.S. Yu, L.M. Dai, *J. Phys. Chem. Lett.* 1 (2010) 467–470.
- [29] C.H. Choi, S.H. Park, S.I. Woo, *J. Mater. Chem.* 22 (2012) 12107–12115.
- [30] D.C. Marcano, D.V. Kosynkin, J.M. Berlin, A. Sinitskii, Z.Z. Sun, A. Slesarev, L.B. Alemany, W. Lu, J.M. Tour, *ACS Nano* 4 (2010) 4806–4814.
- [31] C.H. Choi, M.W. Chung, S.H. Park, S.I. Woo, *RSC Adv.* 3 (2013) 4246–4253.
- [32] C.H. Choi, S.H. Park, S.I. Woo, *Appl. Catal. B Environ.* 119 (2012) 123–131.
- [33] F.T. Thema, M.J. Moloto, E.D. Dikio, N.N. Nyangiwe, L. Kotsedi, M. Maaza, M. Khenfouch, *J. Chem.* 2013 (2013) 150536, doi:10.15115/152013/150536.
- [34] Z.H. Sheng, H.L. Gao, W.J. Bao, F.B. Wang, X.H. Xia, *J. Mater. Chem.* 22 (2012) 390–395.
- [35] G. Nansen, E. Papirer, P. Pioux, F. Moguet, A. Tressaud, *Carbon* 35 (1997) 175–194.
- [36] S.H. Lim, H.I. Elim, X.Y. Gao, A.T.S. Wee, W. Ji, J.Y. Lee, J. Lin, *Phys. Rev. B* 73 (2006) 045402.
- [37] S. Maldonado, S. Morin, K.J. Stevenson, *Carbon* 44 (2006) 1429–1437.
- [38] G. Liu, X.G. Li, P. Ganesan, B.N. Popov, *Appl. Catal. B Environ.* 93 (2009) 156–165.
- [39] A.G. Pandolfo, A.F. Hollenkamp, *J. Power Sources* 157 (2006) 11–27.
- [40] R. Bashyam, P. Zelenay, *Nature* 443 (2006) 63–66.
- [41] L.P. Zhang, Z.H. Xia, *J. Phys. Chem. C* 115 (2011) 11170–11176.
- [42] P.H. Matter, L. Zhang, U.S. Ozkan, *J. Catal.* 239 (2006) 83–96.
- [43] T. Ikeda, M. Boero, S.-F. Huang, K. Terakura, M. Oshima, J.-i. Ozaki, *J. Phys. Chem. C* 112 (2008) 14706–14709.
- [44] A. Ohma, S. Yamamoto, K. Shinohara, *J. Power Sources* 182 (2008) 39–47.
- [45] K.A. Kurak, A.B. Anderson, *J. Phys. Chem. C* 113 (2009) 6730–6734.